Obsidian hydration dating by infrared transmission spectroscopy

Fernando Franchetti, Gustavo Neme, Adolpho Gil, M. Laura Salgan, *IDEVEA-CONICET, FFYL-UNCUYO, Argentina*

Alexander K. Rogers, *Maturango Museum (emiterus), Ridgecrest, California*

James Davenport, *University of Missouri Research Reactor, Columbia, Missouri*

Raven Garvey, *Museum of Anthropological Archaeology, University of Michigan, Ann Arbor, Michigan*

Olga Trofimova, *The Center for Integrated Research, The College of William and Mary, Williamsburg, Virginia*

Thegn N. Ladefoged, University of Auckland, Anthropology, and Te Pūnaha Matatini, Auckland, New Zealand

Christopher M. Stevenson, *School of World Studies, Virginia Commonwealth University, Richmond, Virginia*

Corresponding author: Christopher M. Stevenson, cmstevenson@vcu.edu

Abstract

The obsidian dating method converts the quantity of diffused molecular water within a near-surface hydration layer to elapsed time using an experimentally derived diffusion coefficient predicted from the structural water content of the glass. Infrared spectroscopic transmission measurements on transparent archaeological samples record vibrational responses of water bands in the near infrared region, permitting determination of structural water content (OH) and the amount of ambient diffused water (H_2O). In this application the H_2O water band at 5200cm^{-1} is measured directly. The accuracy of the approach is assessed by an evaluation of the precision of each contributing variable. The new protocol is evaluated using obsidian from radiocarbon dated deposits from Salamanca Cave in Argentina.

KEYWORDS: rhyolite, diffusion, water content, infrared, error analysis, dissolution

INTRODUCTION

The obsidian hydration dating method for archaeology was developed in the late 1950's (Friedman and Smith 1960). It was based on the preparation of a geological thin section for the measurement of hydration layer thickness by high magnification (600x-1000x) optical microscopy. Conversion of the layer to age relied principally on external calibration with

independent dating methods such as radiocarbon. A great leap forward occurred in the 1970's when Friedman and Long (1976) published their classic paper on high temperature (95-250°C) laboratory hydration rate development that sought to establish a compositional basis for the variation in obsidian hydration rates for different geological deposits. Their equation known as the Chemical Index [Hydration Rate= SiO_2 - 45(CaO + MgO) - $20H_2O^+$] (oxides in weight percent) was directed toward bridging this gap in understanding. Further evaluation of the compositional dependence of water diffusion in obsidian (Stevenson et al. 1998) proposed no consistent influence of anhydrous chemistry on the ambient (~20°C) hydration rate. At higher temperatures near the glass transition (~800-1000°C), Zhang and Behrens (2000) and Behrens and Nowak (1997) also found the effect of anhydrous chemistry to be weak, although Karsten et al. (1982) reported that Ca^{2+} concentration may influence hydration rate to a very slight extent.

Obsidian structural water, on the other hand, has a profound effect on hydration rate, which varies directly with water content concentration at both ambient and elevated temperatures (Behrens and Nowak 1997; Lapham et al. 1984; Stevenson et al. 1998; Stevenson and Novak 2011; Zhang and Behrens 2000). Various research efforts have developed a variety of experimental protocols for hydration rate development (Ambrose et al. 2004; Ambrose and Novak 2012; Anovitz et al. 2008; Rogers and Duke 2011, 2014; Rogers and Stevenson 2017; Stevenson et al. 1998). Elevated temperature (≤250°C) diffusion coefficients allow the estimation of the hydration rates at lower archaeological temperature (~10-35°C) through extrapolation using the Arrhenius equation and these data have allowed rate prediction equations to be developed based upon structural water content in the bulk glass (Stevenson et al. 2021).

The method development proposed here for obsidian hydration dating is based upon measuring the two species of water in the bulk matrix of obsidian, and the amount of diffused water in the near-surface hydration layer. The total structural water content of obsidian is H_2O_t = OH + H_2O_{ms} (where OH is structural hydroxyl content and H_2O_{ms} is structural molecular water) and this quantity is measured for the interior *unhydrated* portion of the artifact to be dated. The amount of H_2O_t is used to estimate the hydration rate for surface diffused molecular water. Structural water contains both hydroxyl and molecular water, but hydroxyl is the dominant species of H_2O_t <~ 0.3 wt% and H_2O_{ms} is in fact not detectable by standard commercial infrared spectroscopy at this low concentration. Ambient water diffusion into the artifact surface occurs in the form of molecular water (H_2O_{dm}). Determining a chronometric age estimate for an obsidian artifact is based on measuring the quantity of diffused molecular water that has accumulated since the time the artefact was humanly created from a geological specimen.

The measurement of diffused molecular water (H_2O_{dm}) that forms the hydration layer has been conducted by many different methods that include optical microscopy (Friedman and Smith 1960), resonant nuclear reaction (Lanford 1979), secondary ion mass spectroscopy (Ambrose and Novak 2012; Liritzis 2006; Novak and Stevenson 2012; Riciputi et al. 2002), and infrared photoacoustic spectroscopy (Stevenson et al. 2001, 2013). In this paper, we illustrate the use of infrared *transmission* spectroscopy to determine the concentration of structural water (H_2O_t=OH+H_2O_{ms}) and diffused molecular water (H_2O_{dm}) in the obsidian artifact. This infrared obsidian hydration dating (IR-OHD) approach, that simply passes a beam of light through the artifact, has not been used previously because the surface irregularity of flakes has been perceived as incompatible with an accurate sample thickness measurement necessary for

determining structural water concentration. However, for the many small flakes and blade fragments with near-parallel surfaces that are 0.4-1.0mm thick, we have developed simple aperture methods where these problems are minimized. Another advantage of the method is that the quantity of diffused molecular water forming the hydration layer is quantified by absorbance values and a conversion to weight percent concentration or hydration layer thickness is not required for age estimation.

THE MEASUREMENT OF WATER IN ARCHAEOLOGICAL OBSIDIAN

The methodology presented here requires the measurement of obsidian structural water (H_2O_t = OH + H_2O_{ms}) of the unhydrated glass artifact and the amount of near-surface diffused water (H_2O_{dm}) accumulated since the time of artifact manufacture. These distinct water species (OH and H_2O) are expressed at different locations within the near and mid-infrared spectral regions (450-6000cm^{-1}) (von Aulock et al. 2014). Hydroxyl (OH) exhibits a vibrational peak at 4500cm^{-1} (Figure 1) while total water is represented by a combination band at 3570cm^{-1} (not shown) that reflects the vibrational responses of both OH and H_2O_{ms}. Near-surface diffused water (H_2O_{dm}) is molecularly identical to structural water (H_2O_{ms}) and is incorporated into the combination band at 3570cm^{-1} during the diffusion process. As a result, individual water species, important to this analysis, cannot be distinguished. Molecular water (H_2O_{ms}/H_2O_{dm}) also exhibits an absorption band at 5200cm^{-1} (Figure 1). The band is vibrationally weaker but can be measured with our current instrumentation.

For glass with H_2O_t < ~0.3 wt% the structural water occurs entirely as hydroxyl (Ihinger 1999; Stevenson et al. 2018) and it can be measured with the 4500cm^{-1} water band. The H_2O_{dm} band at 5200cm^{-1} represents diffused water and can be converted to an age before present since no interfering structural H_2O_{ms} is present within the obsidian. We discuss the strengths and weaknesses of this approach below.

It is very important to note at this point, that the methodology in this paper is applied only to obsidians that have <~0.3%H_2O_t so that structural molecular water (H_2O_{ms}) is not present and does not interfere with the measurement of diffused molecular water (H_2O_{dm}) at 5200cm^{-1}. If H_2O_{ms} is a component of the total structural water of the unhydrated obsidian then other methods will need to be developed. Fortunately, many obsidians found around the globe are very low in structural water concentration (Stevenson et al. 2018) because of their slow effusive eruptions and extended cooling history.

Measurement of structural water in unhydrated obsidian

Infrared absorbance can be measured either by peak height or peak area on the sample spectrum but we have adopted the use of peak height because of the greater replicability of measurement (Newman et al. 1986). Water species concentration of hydroxyl (OH) in unhydrated obsidian is calculated using the Beer-Lambert law which, in this case, relates the infrared absorbance intensity of the vibrating water species to concentration within the glass matrix:

$$\text{Concentration } H_2O_{\text{species}} = (ABS*18.02)/(t*d*\varepsilon) \quad (1)$$

where: ABS = absorbance intensity quantified by spectrum peak height (dimensionless), 18.02 is the molecular weight of water, t=thickness of the sample in centimeters, d=obsidian density (g/L), and ε is the extinction coefficient, or proportionality constant, in L/(mol*cm). Each parameter is subject to experimental uncertainty, which determines the uncertainty in OH concentration (Newman et al. 1986). Numerical values of ε for each water band used in this analysis are listed in Table 1 Supplemental.

In this application artifact density (g/L) was estimated by the Archimedes immersion method using a heavy liquid (Stevenson et al. 2018). Thickness of the flake sample was measured with a high precision Mitutoyo micrometer with a reported error of ±0.001mm (1μ). The challenging aspect of this analysis is to measure thickness with sufficient precision to keep the analytical error associated with water species quantification to less than 0.05%. Near parallel sided samples that are ~0.4-1mm thick and transparent to light are the preferred type of samples. This is coupled to measurements locations with small diameters (~1.0mm) and allows the goal of precise water determination to be achieved. If the obsidian samples contain abundant microlites and/or banding, as in our case example discussed below, then near-parallel sided samples with one archaeological surface and one flat polished side are required. (In this case, the method is clearly destructive.)

The advantage of the "through the flake" transmission approach to measuring structural OH is that all the variables (ABS, t, d) may be determined non-destructively unless modification of the specimen is required. A standard benchtop Thermo Nicolet iS10 Fourier transform infrared spectrometer (FTIR) with a halogen light source is used to measure the absorbance. A specimen with near-parallel sides is cleaned with ethanol and placed over a 1.0mm aperture plate mounted to the sample plate in the FTIR compartment equipped with a Pike Technologies beam condenser. After a background spectrum is taken, a second spectrum is collected from the artifact in the near/mid infrared region between 2000-6000cm^{-1}. A total of 128 scans per sample are recorded at a scan speed of 0.2cm/sec, a resolution of 32cm^{-1}, and averaged to produce the final spectrum. The absorbance measurements of peak height for all water species are in reference to a straight baseline that links the peak minima (Figure 1).

After the absorbance reading is completed a fine pointed marker pen is used to locate the measurement spot with a tiny smear of ink that covers the aperture opening. The artifact is removed from the sample plate and the thickness measured with the micrometer. The tips of the micrometer are pointed and finely machined to a diameter of 0.3mm and a built-in pressure clutch determines the final contact pressure. In this manner, lateral variation in sample thickness is minimized. To determine an error factor, we completed 10 repeat measurements on three artifacts and computed the mean and standard deviation. In each case the precision was 0.006cm (6μ) or less. It should be noted that some obsidians have rougher surfaces (Liritzis et al. 2008; Laskaris et al. 2017) and thus separate precision estimates should be established for glasses that are not smooth and glassy.

The hydration rate is a function of temperature modeled by the Arrhenius equation

$$k = A*\exp[-E/(R*T)] \quad (2)$$

where: A is the pre-exponential (diffusion) constant, E is activation energy (J/mol), T is absolute temperature (Kelvin), and R is the universal gas constant [8.314] (Levine 2002:554-556). For high temperatures and pressures (T ~ 1000K, P ~ 0.5 gPa) both the activation energy and the diffusion constant are functions of total water content (Zhang 2008:243). This also applies to hydration at ambient conditions although the equations described by Zhang for higher temperatures do not scale correctly to archaeological conditions. Therefore, an equation for archaeological conditions was empirically derived by Rogers and Stevenson (2022) which correctly describes hydration rates at lower temperatures. Analysis of hydration rate variations over the Holocene, based on temperature proxy data, have shown that the effects of ambient environmental variations are negligible (Rogers 2010, 2015). In the method analyzed here, the diffusion constant is represented by the rate in ABS^2/year at 160°C (433.15K), k_{160}, calculated from the increase in peak height of the 5200cm^{-1} H_2O band with increasing hydration time. The accelerated rate is adjusted to archaeological temperature using the equation:

$$k = k_{160} * \exp\{(-E/R) * [1/423.15 - 1/EHT]\} \quad (3)$$

where: EHT is the effective hydration temperature in K of the archaeological site and the other variables are as defined above. For obsidian at typical archaeological conditions, a change of 1°C creates a change of approximately 6% in EHT. For In this analysis the term k_{160}, which is a function of temperature, is referred to as the "accelerated hydration rate" to distinguish it from the pre-exponential (diffusion constant), which is not a function of temperature over typical archaeological temperature ranges.

In summary, the fundamental principle of the new method is to first measure the OH content of a specimen by FTIR, then use the OH% concentration value to compute the activation energy and accelerated hydration rate from calibration equations (Stevenson et al. 2021), and finally, to compute the archaeological hydration rate from equation (3). Subsequently, the quantity of diffused molecular water of an archaeological specimen is determined by the measurement of the 5200cm^{-1} $H2O_{dm}$ water band peak heights. The age of the specimen is then computed from the absorbance of the 5200cm^{-1} peak using the laboratory rate adjusted to the temperature of the archaeological site.

SALALMANCA CAVE: ARCHAEOLOGICAL CASE EXAMPLE

Archaeological context

Salamanca Cave is located in the semi-arid region of Mendoza, Argentina (Figure 2a, Figure 2b). The archaeology of southern Mendoza has focused on a biogeographic research agenda over the last 20 years where more than 100 archaeological sites from the highlands, piedmont, and lowlands have been investigated (Gil et al. 2022). The research questions of this investigation address the relationship between the first human occupations and megafauna, and an increased demography in the late Holocene which triggered the occupation of marginal environments, technological innovations, and in some places the adoption to agriculture (Neme et al. 2022). Salamanca Cave is a well-preserved context that had the potential to address these questions plus the evaluation of the hypothesized mid-Holocene hiatus through the application of the obsidian hydration dating method.

In 2010, a 2 m x 1 m test unit (A-1) was excavated. The test unit was placed close to the western wall of the cave. The excavation unit was subdivided into two 1m x 1m subunits (Figure 2c). Twenty, 5cm thick arbitrary excavation levels that followed the slope of the cave floor were removed and screened. Excavation continued until the bedrock surface of the cave was encountered. The sediments were a fine loam with little rock content but several small blocks from the cave ceiling were encountered within the matrix. Several bioturbated features were identified (e.g., rodent tunnels) along with several humanly constructed features such as hearth and trash deposits. These bioturbated features became a hindrance to interpreting the stratigraphic record and difficulties were encountered when trying to reconstruct the depositional sequence. The twenty arbitrary levels were collapsed into five stratigraphic units (1-5 from top to bottom) using the natural levels defined from sediment color and texture. The northeast corner of the excavation was the least disturbed and exhibited the most vertical layering. The units were described by grain size, sedimentary structure, and Munsell soil color.

Twelve radiocarbon dates were obtained on carbon samples removed from each stratigraphic unit (Neme at al. 2021). The uncalibrated assays ranged in age from 1,055 to 7,335 ^{14}C years B.P. In the evaluation of the stratigraphy and the radiocarbon dates, three archaeological components (A, B, C) were defined. The youngest component (A) dated to between 1,055 and 1,516 ^{14}C years B.P. The middle component (B) includes the first half of the Stratigraphic Unit 4 where the radiocarbon dates ranged from 1,561 to 2,200 ^{14}C years B.P (Neme at al. 2021:6, Table 2). There was not a sedimentary distinction between this component and lower deposits. However, the presence of two much older radiocarbon dates in component C (7,100 and 7,400 ^{14}C years B.P), and differences in projectile point shape, raw materials, exploited taxa and absence of pottery (Neme et al. 2021) led to the recognition of component C.

Also identified in the first 10cm of the deposit was evidence of activity in the recent past (AD 1600-1800) in the form of hearths associated with domestic fauna (*Capra hircus*), and industrial glass. Although the Spanish colonization in Mendoza began in the 16th century, the expansion of the colonial domain towards the South, where Salamanca cave is located, occurred later; specifically, at the beginning of the 19th century with the foundation of the San Rafael fort in 1805 (Lagiglia 1983) and the installation of the first colonizers. This allowed the local hunter-gatherers to continue with their traditional lifeways despite the Mapuche expansion and the displacement of *puelches* and *pehuenches* ethnicities (Durán 2000). Previous work has shown a coexistence in the use of prehispanic technology, such as lithics and ceramics, with evidence of domestic taxa and some elements of European technology (Gil et al. 2006). This is consistent with the appearance of obsidian artifacts in later historical contexts in Salamanca cave. We did not apply radiocarbon dating to the first five levels (0-25cm) due to the presence of domesticated fauna and European artifacts which defined the use period for the latest occupation of the cave.

A summed probability curve was completed using the radiocarbon calibrated dates from the cave. The distribution was a bimodal curve with both Early and Late Holocene occupations. The curve also identified a significant temporal hiatus that includes most of the Middle Holocene and the Early-Late Holocene from 2,400 to 7,400 cal. years B.P. This pattern correlates with occupations present within two other cave sequences (El Manzano and Huenul) within the Andean Piedmont (Neme et al. 2021; Barberena et al. 2015).

Obsidian hydration dating

In order to evaluate the ability of infrared obsidian hydration dating (IR-OHD) to provide chronometric dates that correlate with radiocarbon assays an evaluation exercise was conducted using obsidian artifacts recovered from the stratigraphic deposits at Salamanca Cave (Table 1). The altered stratigraphy of the cave and the lack of obsidian flakes in direct association with radiocarbon samples prevented the examination of a one-to-one correspondence between the two sample outcomes. Instead, we determined that a successful result would be achieved if the obsidian dates spanned the same range as the radiocarbon ages and identified the mid-Holocene abandonment of this region.

Fifteen flake samples were selected from the recovered assemblage that were close to being parallel sided. These samples were analyzed by X-ray fluorescence at the University of Missouri Research Reactor and compared with the central Argentina trace element data base (Giesso et al. 2011; Salgán and Pompei 2017).

Sample preparation for dating involved grinding one side of the flake flat on a lapidary wheel with aluminum oxide grit and then dry polished with abrasive papers to an 800-grit reflective finish on a rotary wheel. The samples were cleaned with ethanol. Spectroscopic measurements were made on the Thermo Nicolet iS10 spectrometer. The $5200cm^{-1}$ H_2O_{dm} band and the $4500cm^{-1}$ hydroxyl band (Figure 1) were collected

APPLICATION OF THE EXPERIMENTAL METHOD AS MODELED

The first step in the method is to determine the OH content (wt%) of the specimen, using the absorption band at $4500cm^{-1}$. Hydroxyl content is computed by the Beer-Lambert law (Equation (1) above) using the specimen density (d), thickness (t) and its absorbance at $4500cm^{-1}$ (A_{4500}). The parameters required to compute hydroxyl content and its accuracy are summarized in Table 2 Supplemental. Then, the accumulation of diffused molecular water is measured by taking a peak height measurement of the $5200cm^{-1}$ H_2O_{dm} band.

Analysis method

As shown by equations (2) and (3), computation of a hydration rate requires determining the activation energy E and the accelerated hydration rate (k_{160}) at 160°C, both of which are functions of OH content. The activation energy equation employed here is:

$$E = 24{,}293 + 71{,}277*\exp(-1.41*OH) \quad (6)$$

where: E is in J/mol and OH is in wt.%. Activation energy can also be expressed in terms of kelvins by dividing by the universal gas constant yielding:

$$Q = 2{,}922 + 8{,}572*\exp(-1.41*OH) \quad (7)$$

where: Q = E/R, with R as the universal gas constant. Equation (6) is from Stevenson et al. (2021: 9, Supplemental eq. 9), recomputed to omit four anomalous data points: Gabelotto, Takayama 054, Great Barrier, and Coso Site 2. The original equation had root mean square (rms) residuals of 1971 J/mol (N = 20). The points were excluded judgmentally based on excessively-large scatter; omitting these points reduced the rms residuals to equation (6) above by nearly a factor of two to 1033 J/mol (N = 16) and $R^2 = 0.9951$, while still retaining an adequate sample size. Figure 1 (Supplemental) shows the quality of the fit.

Accelerated hydration rate (k_{160}) for the 5200cm^{-1} band were computed by a least-squares best fit to absorbance data derived from accelerated hydration at 160°C for five geochemical sources with OH < ≈0.3 wt%. Data used for the fit are presented in Table 3 Supplemental and plotted in Figure 1 Supplemental.

Selection of the form for the best fit equation for the hydration rate was based on the physics of glass and its expected behavior under hydration. Obsidian is a rhyolitic glass, having a tetrahedral matrix of silica (SiO_2) and alumina (Al_2O_3), with alkali metal and alkali earth ions in the interstices to provide charge balance (Shelby 2005). The interatomic spacing of the matrix is approximately 0.087 angstroms (Doremus 2002:67). Hydroxyl (OH) is created in the form of SiOH by a chemical reaction between the matrix atoms and water molecules. Each time the SiOH reaction occurs it breaks an Si – O bond and creates a local void, so the OH concentration is a proxy measure of the porosity or openness of the glass matrix. The smaller the intrinsic OH concentration, the smaller the number of such voids. However, diffusion can still occur even when OH = 0, via what Kuroda et al. (2018) referred to as "normal" diffusion. Thus, any best fit line between k_{160} and OH concentration will not pass through the origin, and, in fact, must have a y-intercept > 0. Further, increasing the OH concentration is equivalent to increasing the number of voids or fast pathways, which suggests the hydration rate should increase with OH (Kuroda and Tachibana 2019), and a linear increase was assumed. A linear least-squares best fit to the data set is:

$$k_{160} = 0.1164*OH + 0.0018 \quad (8)$$

in which k_{160} is in units of $(ABS_{5200})^2$/year. The fit, shown in Figure 1 (Supplemental), is good, with $R^2 = 0.9808$ and rms residuals of 0.0018.

The complete form of the equation for hydration rate at any temperature T (in K) and OH (in wt%) is then:

$$k = (0.1164*OH + 0.0017) *\exp \{[2{,}922 + 8{,}572*\exp(-1.41*OH)]* (1/423.15 - 1/T)\} \quad (9)$$

The units of k are $(ABS_{5200})^2$/yr. The range of validity for this equation is $0.09 \leq OH < 0.27$ wt%.

Effective hydration temperature (EHT)

A dynamic model was used to compute effective hydration temperature (EHT) for the cave site based on digital temperature data of the soil deposits. The temperature dependence of the

hydration rate was modeled by the Arrhenius equation (equation (2)), in which temperature is a function of time, since site temperatures vary annually, seasonally, and diurnally. The archaeological hydration rate is found by integrating equation (2) over the course of a full year; the integral is computed as a finite sum over one-year's-worth of temperature data points:

$$k_{eff} = (1/N) * A * \sum[\exp(-Q/T_n)] \quad (10)$$

where: k_{eff} is the effective (or archaeological) rate, T_n is the sequence of temperature data points, and the sum is taken from 1 to N, the total number of data points. By the definition of EHT, we also have:

$$k_{eff} = A * \exp(-Q/EHT) \quad (11)$$

Setting equations (10) and (11) equal, and after some algebra:

$$EHT = -Q/\ln\{(1/N) * \sum[\exp(-Q/T_n)]\} \quad (12)$$

Here EHT is in kelvins, so EHT in Celsius is obtained by subtracting 273.15.

An archaeological site temperature was determined from two Hobo data loggers buried within Salamanca Cave from January 29, 2021 to January 30, 2022. Temperature measurements were made every 4 hours at a depth of 40cm for a total of 366 days. Effective hydration temperature was computed by the method in equation (12) above, using a full year of data points (N = 2190). Since the EHT is a (weak) function of the activation energy of the obsidian, an EHT was computed for three activation energy values, 9500K < Q < 10500K, which brackets the artifact E values from Salamanca Cave. Table 4 Supplemental shows the results, with annual average temperature included as a check. Combining the data from the two sensors yields an EHT of 16.11 ± 0.095 °C or 289.26 K. The standard deviation increases the uncertainty in the resulting age by only ≈ 1.1%, so it is considered negligible.

Clearly temperature conditions have varied over the course of the Holocene. However, obsidian hydration is a very slow process, and analysis of the effects of such variation using temperature proxy data have shown the effects on OHD-computed age to be negligible (Rogers 2010, 2015).

Relative humidity (RH)

Soil relative humidity less than 100% can lower the diffusion coefficient (Friedman et al. 1994; Mazer et al. 1991). Therefore, a Hobo relative humidity sensor was placed at a depth of 40cm below the surface. Soil humidity was logged at 4-hour intervals over the 366-day exposure period. In the first month the %RH values were well below the annual trend, because Test Unit A-1 was re-excavated to insert the sensor into the soil profile and the soil moisture of the refilled trench required a month to equilibrate with the surrounding atmosphere. Relative humidity at depth was computed after equilibration using the data stream from the sensor, yielding RH = 72.58 ± 0.78 % (N = 2029, CV = 0.01).

The impact of RH on the obsidian hydration rate was experimentally addressed by Mazer et al. (1991). They demonstrated that the hydration rate drops rapidly as the %RH declines from 100% to 90% after which the impact is minimal. Therefore, the decline is not linear and using their data, we estimated that the decline in the rate of hydration at 72.58 %RH to be ≈13%. To compensate for the lower relative humidity the diffusion constant in the Arrhenius equation was multiplied by the coefficient RH = 0.87 in equation (13).

Age computation

Finally, the absorbance intensity from the diffused water of hydration (ΔA) is computed from equation (5), with ΔA in units of absorbance units*cm^{-1}, measured by peak height at 5200cm^{-1}, and age is computed:

$$t = \Delta A^2/(k_{160}*RH) \quad (13)$$

where: k_{160} is in (absorbance units *cm^{-1})^2/year and RH has no units.

ANALYSIS OF OH MEASUREMENT ACCURACY

In this section, we analyze and quantify the accuracy of the OH measurement and the resulting effects on accelerated hydration rate, activation energy, ambient hydration rate, and computed age.

Measurement of hydroxyl

By propagation of error theory (Cvetanovic et al. 1979:51ff.; Taylor 1982:173-175), the accuracy of the Beer-Lambert determination of OH content is given by:

$$\sigma_w^2 = \sigma_M^2*[A/(d*t*\varepsilon)]^2 + \sigma_A^2*[M/(d*t*\varepsilon)]^2 + \sigma_d^2*[M*A/(t*\varepsilon*d^2]^2 + \sigma_t^2*[M*A/(d*\varepsilon*t^2]^2 + \sigma_\varepsilon^2*[M*A/(d*t*\varepsilon^2]^2 \quad (14)$$

Table 2 Supplemental shows the parameter values for this case.

Rate and age computation accuracy

By applying propagation of error methods to equation (2), the accuracy of rate k at the archaeological temperature (EHT in kelvins) is:

$$CV_k = \text{sqrt}\{[(\sigma_E/R)*(1/423.15 - 1/EHT)]^2 + CV_{k150}^2 + [(E*\sigma_{EHT}/(R*EHT^2)]^2\} \quad (15)$$

Both E and k_{160} are computed from the OH value, and each therefore has two sources of experimental error: the effects of σ_{OH} on the outcome of the best fit, and the rms (root mean squared) residuals to the best fit. For activation energy E, the rms residuals to the best fit equation are 1033 J/mol. The contribution to σ_E due to OH error is 71277*1.41*exp(-1.41*OH)*σ_{OH}; the CV (coefficient of variation) of rate due to uncertainties in E includes the rms residuals:

$$CV_E = sqrt\{[71277*1.41*exp(-1.41*OH)*\sigma_H]^2 + 1033^2]\} \quad (16)$$

A similar procedure is used to evaluate the error contribution of k_{160} at 5200cm^{-1}. The effect on σ_{k160} due to OH errors is $0.1164*\sigma_{OH}$, so including the rms residuals of 0.00118 gives

$$CV_{k160} = sqrt[(0.1164*\sigma_{OH})^2 + 0.00118^2]/k_{160} \quad (17)$$

The third term on the right in equation (15) is computed for an EHT of 16.11°C (derived above). The EHT computation was based on a dynamic model of the hydration process, using actual sensor data as an input, and $\sigma_{EHT} = 0.095$°C. Uncertainty arises because the data are for a single year, so there is a question of representativeness. We estimate the overall uncertainty in EHT to be $\sigma_{EHT} = 0.5$°C. Thus, the contribution of EHT to hydration rate uncertainty is:

$$CV_{EHT} = (5.98 \times 10^{-6})*[2{,}922 + 8{,}572*exp(-1.41*OH)] \quad (18)$$

and the CV of hydration rate is:

$$CV_k = sqrt(CV_E^2 + CV_{k150}^2 + CV_{EHT}^2) \quad (19)$$

Finally, the accuracy of age is:

$$CV_t = sqrt[(2*CV_A)^2 + CV_k^2] \quad (20)$$

Here $CV_A = \sigma_A/\Delta A$, with ΔA defined by equation (5). Newman et al. (1986:1533) conducted repeatability measurements at 3570cm^{-1} and concluded that differences seldom exceeded 0.015 absorbance units; converting this estimate to standard deviation yields $\sigma_A = 0.0014$, so the age standard deviation σt is:

$$\sigma_t = t*sqrt[(0.0028/\Delta A)^2 + CV_k^2] \quad (22)$$

where t is the age and CV_k is defined by equation 19).

Thus, to compute an age, the absorbance at 5200cm^{-1} and at 4500cm^{-1} is measured on the archaeological specimen and converted to ΔA by equation (5). The absorbance at 4500cm^{-1} is converted to OH% used to compute E and k_{160}, from which the rate is computed, and an age is estimated by equation (13). The standard deviation of this age is given by equation (22).

NATURAL TRANSFORMATIONS TO THE OBSIDIAN SURFACE

Within the context of this analysis, our hydration rate development experiments revealed that after vapor reaction in a stainless steel cannister for 64.79 days at 160°C the surface of the Las Cargas obsidian sample was irregularly corroded while a sample of Laguna del Maule glass exposed to the same conditions maintained its surface integrity and did not show any evidence of corrosion or pitting at high magnification (500x). This observation suggested to us that the hydrated sample of Las cargas obsidian was a low durability glass sample which had the

potential to be altered in archaeological context over time by surface dissolution. As a result, the progressive loss of the developing surface hydration layer could result in non-representative hydration and obsidian dates that would be too recent.

Surface dissolution has been documented on obsidian artifacts that come from soils that are alkaline (Ambrose 1976) with a pH of 8.0 or greater. The effect is most noticeable when the surface of the artifact is covered in shallow pits or channels. While a full treatment of glass surface dissolution is complex and beyond the scope of this paper, we inspected each artifact for surface damage with a Hirox RH-2000 digital microscope using the high-range lens at magnifications of 350x and 500x under direct light illumination. The Hirox system has a multi-focus capability that can create a single in-focus image from an uneven flake surface. We then examined each of the artifacts from Salamanca Cave for the presence of surface corrosion.

RESULTS

The XRF analysis revealed that nine of the artifacts originated from the Las Cargas obsidian source, two from the Zaino source, one from Laguna del Maule and one from Paramillos (Table 1, Figure 2 Supplemental). Two flakes were too small and thin for analysis.

A pH test on soil from within Salamanca cave was conducted and returned a value of 6.88 which is a near neutral in terms of soil acidity. Under these conditions surface dissolution has a low probability of occurrence. The inspection of the artifact surfaces with the Hirox microscope indicated that only one of the fourteen artifacts (RBC-893) had identifiable pits characteristic of surface dissolution (Table 1). Figure 3 Supplemental (top) shows an artifact without evidence of surface pitting while Figure 3 (bottom) shows the pitting and channels associated with surface dissolution. This sample was not considered in the final analysis.

Table 7 Supplemental presents the absorbance measurements and specimen parameters for this data set. Hydroxyl content, based on absorbance at 4500cm^{-1}, was computed by equation (1) and its standard deviation was computed by equation (15) from the parameter values in Tables 2 Supplemental. The results are in Table 5 Supplemental (last two columns). Hydroxyl content was then used to compute E and k_{160} by equations (6) and (8). The hydration rate at archaeological temperature was computed by equation (9) and a known value of EHT. The ages were then computed by equation (15), and the standard deviation of age by equation (23). The results are presented in Table 7 Supplemental.

The obsidian hydration dates using the k_{160} accelerated rate and the 5200cm^{-1} absorbance values are in Table 7 Supplemental. They range in age from 149±23 BP to 2202±387 BP. Nine of the samples are before 1090±189 BP and five form a small group between 1090±189 and 2202±387 BP. None of the dates fall within the Middle Holocene and they do not extend into the Early Holocene.

DISCUSSION

In this paper, we have presented an approach to obsidian hydration dating where the measurement of obsidian structural water (OH) and diffused ambient water (H_2O_{dm}) was

determined by transmission spectroscopy can be applied to the archaeological obsidian dating process. Natural glass studies over the last few decades that focus on rhyolites consistently point to the fact that total structural water is the most influential variable in determining the rate of hydration and we have used this insight as a basis for predicting the magnitude of the diffusion coefficient in archaeological obsidians.

Recent studies of water diffusion in glass support the premise of our dating calibrations and have a sound theoretical footing. Obsidian is a rhyolitic glass, having a tetrahedral matrix of silica (SiO_2) and alumina (Al_2O_3). Hydroxyl (OH) is created in the molten state in the form of SiOH by a chemical reaction between the matrix atoms and water molecules. Each time the SiOH reaction occurs, it breaks an Si – O bond and creates a local void or pathway for molecular water diffusion. The OH concentration is a proxy measure of the porosity or openness of the cooled glass matrix which correlates with the magnitude of the diffusion coefficient.

Measuring the critical parameters of OH and diffused surface water (H_2O_{dm}) at high levels of precision is required. In the recent past, infrared photoacoustic studies have been used to measure these critical parameters (Stevenson et al. 2001; Stevenson et al. 2013) and it was initially adopted because the method was insensitive to sample shape irregularity. However, as applied, the instruments limited range could not measure the water band at 5200cm^{-1} and lacked the potential non-destructive capability of the transmission approach.

The method presented here uses FTIR spectroscopy to monitor the energy absorbance of two vibrational peaks (4500cm^{-1} and 5200cm^{-1}) as the infrared beam passes through the obsidian sample. The analytical strength of the method is the simultaneous measurement of both water peaks, and when the sample is translucent, and contains few inclusions or banding, artifacts up to ~1.5 millimeters thick can be measured. We have also developed the necessary calibration curves for the activation energy and accelerated rate, and have applied a dynamic model from soil thermal monitoring to compute effective hydration temperature.

In order to estimate the accuracy of the OHD ages, we have also presented a mathematical analysis of the error sources affecting the computation. Figure 4 shows the contribution of each variable. Examination of Figure 4 shows that the primary uncertainty arises from the equations relating activation energy E to OH content (equations (6) and (7) above), and that the uncertainty arising from activation energy (CV_E) is generally twice the magnitude of the uncertainty from k_{160} or EHT. The errors in E are magnified since activation energy occurs in the exponential in equations (2) and (9). These errors are caused by uncertainties in OH itself (σ_{OH}) and by the rms residuals to the best-fit equation, with the residuals being by far the larger contributor. If the quality of the best-fit were improved to reduce the residuals to essentially zero, the age accuracy would be improved by a factor of two. Errors in the accelerated rate are smaller because they do not occur within the context of an exponential. Errors in EHT are also much less significant because EHT was computed from actual temperature data by a dynamic model (equation (12)), although the question of whether the year-long run of temperature data truly represents long-term archaeological time-spans remains.

Finally, errors introduced by FTIR measurement of diffused water accumulated by hydration are small. However, an important caveat on sample transparency needs to be

emphasized here. The quality of the water bands at 4500cm^{-1} and 5200cm^{-1} in terms of their form are impacted by the presence of microlites, voids, and flow banding that can either block transmission of infrared light or scatter the light so that the energy does not reach the instrument detector (von Aulock et al. 2014). Distortions to the shape of the peaks can occur, especially to the minima of the 4500cm^{-1} peak which will not have a clean transition to the baseline but exhibit an extended slope that trails off towards higher or lower wavenumbers (See Figure 1). Thus, the peak height measurement becomes difficult to constrain. Therefore, highly transparent samples are required and this may entail the use of very thin samples or the grinding of samples to get the required clarity. One must be aware that as the sample becomes thinner the hydroxyl peak height is also smaller.

The ages derived from this application generally agree with the radiocarbon dates from the cave site (Figure 3). Of particular importance is that the variation of OHD ages probably represents an actual spread in terms of the time of artifact manufacture and use, and not simply uncertainty. In classic OHD using optical microscopy there is no control for intrinsic water variations within an obsidian source, which makes a significant contribution to age standard deviation. However, here OH content was measured directly, which controls for water content variation, so the spread in ages is probably real.

Our IR-OHD results hint at the presence of a regional hiatus for southern Mendoza as identified by radiocarbon dating. All of the 14 obsidian dates (one was excluded because of surface pitting) are before the period of the proposed hiatus that begins around 2500BP and no dates occur earlier in time. This may also be due to our small sample size or the way obsidian was curated by the cave inhabitants. Only two radiocarbon dates are older than 7000 years BP and both come from the bottom layers (Levels 19 and 20). It means that the older human occupations are scantily represented in the cave, making it more difficult to obtain cultural remains associated with these ages (Neme et al. 2021). Other researchers concerned with the chronology of the southern Mendoza region (Garvey and Bettinger 2018) argue for a continued human use of the landscape in their application of OHD. Our small sample size in this analysis is insufficient to settle the question of a Middle Holocene hiatus but with proper application it could be an effective tool in helping to resolve the debate. One component of that proper application is being aware that obsidian surface dissolution is potentially a problematic variable. Surface dissolution is solution activated and requires direct water contact with the artifact (Declerque et al. 2013). The interior of Salamanca Cave is for the most part protected from rainfall and the documented relative humidities are low. Thus, the probability of artifact surface dissolution from contact with underlying groundwater is low. Artifacts buried within open sites such as the nearby site of El Desecho, even in semi-arid areas are periodically in contact with ground waters and this may in the long-tern initiate dissolution at the micron scale if the soil pH is outside the neutral range. Artifacts scavenged from such contexts and then brought to the cave may account for the one altered sample that we encountered.

CONCLUSIONS

We have presented a method for computing ages of obsidian artifacts, based on an transmission spectroscopy measurement method, with the necessary calibration curves for activation energy and accelerated rate and a dynamic model to compute effective hydration temperature. We have

also presented a comprehensive analysis of accuracy to determine the standard deviation of the age estimate, whose results can be applied in other contexts employing the method. Finally, we have shown partial agreement with radiocarbon dates from the Salamanca Cave site. The error analysis methodology developed here is widely applicable to OHD studies beyond Salamanca Cave.

ACKNOWLEDGEMENTS

This archaeological research on this project was generously supported by *IDEVEA-CONICET, FFYL-UNCUYO,* Argentina. Fundamental laboratory research was made possible by the Marsden Award (Contract: UOA1619), New Zealand, for which we are highly appreciative. Similarly, we are very thankful to the Archaeometry Laboratory at MURR which is supported by the National Science Foundation (Award No. 2208558). We are also grateful to the Sagal family, the owner of the cave, who kindly hosted us during the different fieldwork sessions at the site.

DATA AVAILABILITY STATEMENT

All relevant datasets produced in this study are provided as supplemental documents linked to the manuscript. The XRF data can be downloaded from the MURR Archaeometry Laboratory data repository at: https://archaeometry.missouri.edu/murr_database.html

ORCID

Christopher M. Stevenson https://orcid.org/ 0000-0002-3575-2363

REFERENCES

Ambrose, W. (1976). Intrinsic hydration rate dating of obsidian. In: R.E. Taylor (Ed.), *Advances in Obsidian Glass Studies*. Hide Park, Noyes (pp. 81–105), New Jersey.

Ambrose, W., Novak, S.W., & Abdelrehim, I. (2004). Powdered obsidian for determining hydration rates and site thermometry. *Mediterranean Archaeology and Archaeometry*, *4,* (2), 17-32.

Ambrose, W., Novak, & S.W. (2012). Obsidian hydration chronometrics using SIMS and optical methods from 26-year temperature-controlled exposures. In: I. Liritzis and C.M. Stevenson (Eds.), *Obsidian and Ancient Manufactured Glasses (*pp. 15-25), University of New Mexico Press, Albuquerque.

Anovitz, L.M., Cole, D., & Fayek, M. (2008). Mechanisms of rhyolitic glass hydration below the glass transition. *American Minera*logist, *93,* 1166-1178.

Barberena, R., Hajduk, A., Gil, A.F., Neme, G.A., Durán, V., Glascock, M.D., Giesso, M., Borrazzo, K., de la Paz Pompei, M., Salgán, M. L., Cortegoso, V., Villarosa, G., & Rughini, A. A. (2011). Obsidian in the south-central Andes: Geological, geochemical, and archaeological assessment of north Patagonian sources (Argentina). *Quaternary International, 245*, 25-36.

Barberena R. (2015). Cueva Huenul 1 archaeological site (northwestern Patagonia, Argentina): initial colonization and Middle Holocene demographic retraction. *Latin American Antiquity, 26*, 304–318.

Behrens, H. & Nowak, M. (1997). The mechanisms of water diffusion in polymerized silica melts. *Contributions to Mineralogy and Petrology, 126*, 377-385.

Cvetanovic, R. J., Singleton, D. L., & Paraskevopoulos, G. (1979). Evaluations of the mean values and standard errors of rate constants and their temperature coefficients. *Journal of Physical Chemistry, 83*, (1), 50-60.

Declerque, J., Diedrich, T., Perrot, M., Gislason, S.R., & Oelkers, E.H. (2013). Experimental determination of rhyolitic glass dissolution rates at 40–200ºC and 2 < pH < 10.1. *Geochimica et Cosmochimica Acta, 100*, 251-263.

Doremus, R.H. (2002). *Diffusion and Reactive Molecules in Solids and Melts*. Wiley Interscience, New York.

Durán, V. (2000). Poblaciones indígenas de Malargüe: su arqueología e historia. CEIDER, Serie libros Nº 1. Facultad de Filosofía y Letras, Universidad Nacional de Cuyo, Mendoza.

Friedman, I., & Smith, R. (1960). A new dating method using obsidian; Part 1, the development of the method. *American Antiquity, 25*, 476-493.

Friedman, I., & Long, W. (1976). Hydration rate of obsidian. *Science, 159*, 347-352.

Friedman. I, Smith, F., & Smith, G. (1994). Is obsidian dating affected by relative humidity? *Quaternary Research, 41*, 185-190.

Garvey, R., & Bettinger, R. (2018). A regional approach to prehistoric landscape use in west-central Argentina. *Journal of Archaeological Science Reports, 19*, 846-855.

Giesso, M., Durán, V., Neme, G.A., Glascock, M.D., Cortegoso, V., Gil, A.F., & Sanhueza, L. (2011). A study of obsidian source usage in the Central Andes of Argentina and Chile. *Archaeometry, 53*, (1), 1-21.

Gil, A., Neme, G., & Durán, V. (2006). Explotación faunística e incorporación de ganado doméstico euroasiático: el registro arqueológico en la frontera Nordpatagónica. *Comechingonia. Revista de Arqueología, 9*, (1), 5-18.

Gil, A. F., Peralta, E. A., Franchetti, F. R., & Neme, G. A. (2022). Estructura ambiental y dinámica humana en el sur de Mendoza. In Neme, G. and Gil, A. (Eds.) *Arqueología del sur de Mendoza: líneas de evidencia en perspectiva biogeográfica.* Sociedad Argentina Antropología.

Glascock, M.D. 2020. A systematic approach to geochemical sourcing of obsidian artifacts. *Scientific Culture* 6, (2), 35-47.

Kuroda, M., Tachibana, S., Sakamoto, N., Okumura, S., Nakamura, M., & Yurimoto, H. (2018). Water diffusion in silica glass through pathways formed by hydroxyls. *American Mineralogist*, *103*, 412–417.

Karsten, J., Holloway, J., & Delaney, J. (1982). Ion microprobe studies of water in silicate melts: temperature-dependent water diffusion in obsidian. *Earth and Planetary Science Letters, 59*, 420-428.

Kuroda, M., & Tachibana, S. (2019). Effect of structural dynamic property of melt on water diffusion in rhyolite melt. *ACS Earth and Space Chemistry, 3*, (9), 2058–2062.

Lagiglia, H. (1983). Arqueología e historia del fuerte San Rafael del Diamante. En: Morresi y Gutierrez (Eds.), *Presencia Hispánica en la Arqueología Argentina*, Vol.1, UNNE, Resistencia.

Lanford, W., Davis, K., Lamarche, P., Laursen, T., Groleau, R., & Doremus, R.H. (1979). Hydration of soda-lime glass. *Journal of Non-crystalline Solids, 33*, 249-266.

Lapham, K., Holloway, J., & Delaney, J. (1984). Diffusion of H_2O and D_2O in obsidian at elevated temperatures and pressures. *Journal of Non-Crystalline Solids, 67*, 179-191.

Laskaris, N., Liritzis, I., Bonini, M., Ridi, F., Kersting, R., & Al-Otaibi, F. (2017). AFM and SIMS surface and cation profile investigation of archaeological obsidians: New data. *Journal of Cultural Heritage, 25*, 101-112.

Laskaris, N., and Liritzis, I. 2020. Surface and interface investigation of archaeological obsidian artifacts with TOF-SIMS; Case Study. *Scientific Culture 6*, (3), 85-89.

Levine, I. (2002). *Physical Chemistry*. McGraw-Hill, New York.

Liritzis, I. (2006). SIMS-SS: A new obsidian hydration dating method: Analysis and theoretical principles. *Archaeometry, 48*, 533-547.

Liritzis, I., Bonini, M., & Laskaris, N. (2008). Obsidian hydration dating by SIMS-SS: Surface suitability criteria from atomic force microscopy. *Surface Interface Analysis, 40*, 458–463.

Mazer, J.J., Stevenson, C.M., Ebert, W.L., & Bates, J.K. (1991). Hydration of obsidian as a function of relative humidity and temperature. *American Antiquity, 56*, 504-513.

Neme, G., Zárate, M., Pompei, M., Franchetti, F., Gil, A., Giardina, M., Seitz, V., Laura Salgán, M., Abbona, C., & Fernández, F. (2021). Population dynamics and human strategies in northwestern Patagonia – a view from Salamanca Cave (Mendoza, Argentina). *Documenta Praehistorica* XLVIII. DOI: 10.4312\dp.48.15.

Neme, G., Gil, A., Salgan, L., Giardina, M., Otaola, C., Pompei, M. D. L. P., ... & Abbona, C. (2022). A biogeographic approach to farming limits in northern Patagonia, Argentina. *Chungara-Revista de Antropologia Chilena*, *54* (3), 397-418.

Newman, S., Stolper, E.M., & Epstein, S. (1986). Measurement of water in rhyolitic glasses: Calibration of an infrared spectroscopic technique. *American Mineralogist, 71,* 1527-1541.

Novak, S., & Stevenson, C.M. (2012). Aspects of secondary ion mass spectrometry (SIMS) depth profiling for obsidian hydration dating. In: I. Liritzis and C.M. Stevenson (Eds.), *Obsidian and Ancient Manufactured Glasses (*pp. 3-14). University of New Mexico Press, Albuquerque.

Riciputi, L., Elam, M., Anovitz, L., & Cole, D. (2002). Obsidian diffusion dating by secondary ion mass spectrometry: A test using results from Mound 65, Chalco, Mexico. *Journal of Archaeological Science, 29*, 1055-1075.

Rogers, A. (2007). Effective hydration temperature of obsidian: A diffusion-theory analysis of time-dependent hydration rates. *Journal of Archaeological Science, 34*, 656-665.

Rogers, A. (2010). How did Paleotemperature Change Affect Obsidian Hydration Rates? . *Bulletin of the International Association for Obsidian Studies #42, (Winter 2010),* 13 – 20.

Rogers, A. (2012). Temperature correction for obsidian hydration dating, In: I. Liritzis and C. M. Stevenson (Eds.), *Obsidian and Ancient Manufactured Glasses* (pp. 46-55*).* University of New Mexico Press, Albuquerque.

Rogers, A. (2015). A Method for Correcting OHD Age for Paleo-Temperature Variation. *Bulletin of the International Association for Obsidian Studies #52, (Winter 2015),* 6 – 13.

Rogers, A., & Duke, D. (2011). An archaeologically validated protocol for computing obsidian hydration rates from laboratory data. *Journal of Archaeological Science, 38*, 1340-1345.

Rogers, A., & Duke, D. (2014). Unreliability of the induced hydration method with abbreviated hot-soak protocols. *Journal of Archaeological Science, 52*, 428-435.

Rogers, A., and Stevenson, C.M. (2022). An Equation Relating Obsidian Hydration Rate to Temperature and Structural Water Content. *Bulletin of the International Association for Obsidian Studies #69, (Winter 2022),* 3 – 15.

Rogers, A., & Stevenson, C.M. (2017). Protocols for laboratory hydration of obsidian, and their effect on hydration rate accuracy: A Monte Carlo simulation study *Journal of Archaeological Science – Reports, 16*, 117-126.

Salgán, M. L. & de La Paz Pompei, M. (2017). Obsidian source El Peceño: First results of technological, geochemical and spatial approach. *Revista del Museo de Antropología, Suplemento Especial, 1*, 51-58.

Shelby, J. (2005). *Introduction to Glass Science and Technology*, 2nd edition. Royal Society of Chemistry, Cambridge.

Stevenson, C. M., Mazer, J.J., & Scheetz, B. (1998). Laboratory obsidian hydration rates: Theory, method and application. In: M.S. Shackley (Ed.), *Archaeological Obsidian Studies: Method and Theory*. Advances in Archaeological and Museum Science, Volume 3 (pp. 181-204). Plenum Press, New York.

Stevenson, C.M., Abdelrehim, I., & Novak, S.W. (2001). Infrared photoacoustic measurement of obsidian hydration rims. *Journal of Archaeological Science, 28*, 109-115.

Stevenson, C.M., & Novak, S.W. (2011). Obsidian hydration by infrared spectroscopy: method and calibration. *Journal of Archaeological Science, 38*, 1716-1726.

Stevenson, C.M., Ladefoged, T., & Novak, S.W. (2013). Prehistoric settlement on Rapa Nui, Chile: An evaluation of obsidian hydration dating using infrared photoacoustic spectroscopy. *Journal of Archaeological Science, 40*, 3021-3030.

Stevenson, C.M., Rogers, A.K., & Glascock, M. (2018). Variability in obsidian structural water content and its importance in the hydration dating of cultural artifacts. *Journal of Archaeological Science Reports, 23*, 231-242.,

Stevenson, C.M., Rogers, A.K., Novak, S.W., Ambrose, W., & Ladefoged, T. (2021). A molecular model for obsidian hydration dating. *Journal of Archaeological Science Reports 36*, 102824.

Taylor, J. (1982). *An Introduction to Error Analysis.* University Science Books, Mill Valley.

von Aulock, F.W., Kennedy, B.M., Schipper, C.I., Castro, J.M., Martin, D.E., Oze, C., Watkins, J.M., Wallace, P.J., Puskar, L., Bégué, F., Nichols, A.R.L., & Tuffen, H. (2014). Advances in Fourier transform infrared spectroscopy of natural glasses: From sample preparation to data analysis. *Lithos, 206-207*, 52-64.

Zhang, Y. (2008). *Geochemical Kinetics*. Princeton University Press, Princeton.

Zhang, Y., Belcher, R., Wang, L., & Newman, S. (1997). New calibration of infrared measurement of dissolved water in rhyolitic glasses. *Geochimica et Cosochimica Acta, 62,* 3089-3100.

Zhang, Y., & Behrens, H. (2000). H_2O Diffusion in rhyolitic melts and glasses. *Chemical Geology, 169*, 243-262.

SUPPORTING INFORMATION

Additional supporting information can be found online in the Supporting Information section at the end of this article.

Table 1. Salamanca Cave obsidian specimen provenience, geological source and condition

Lab. No. RBC-	Provenience	Obsidian Source	Surface Condition
860	A-1/Niv 14/Sur	Las Cargas	No pitting
862	A-1/Niv 14/Sur	Las Cargas	No pitting
864	A-1/Niv 14/Sur	Las Cargas	No pitting
867	A-1/Niv 15/Norte	Las Cargas	No pitting
868	A-1/Niv 15/Norte	Las Cargas	No pitting
870	A-1/Niv 15/Norte	Zaino	No pitting
871	A-1/Niv 15/Norte	Paramillos	No pitting
876	A-1/Niv 16/Norte	Too small	n/a
877	A-1/Niv 16/Norte	Laguna del Maule-1	No pitting
878	A-1/Niv 17/Norte	Las Cargas	No pitting

881	A-1/Niv 17/Norte	Las Cargas	No pitting
882	A-1/Niv 17/Norte	Zaino	No pitting
883	A-1/Niv 17/Norte	Las Cargas	No pitting
886	A-1/Niv 18/Norte	Too small	n/a
893	A-1/Niv 20/Norte	Las Cargas	Pitted

List of Figures

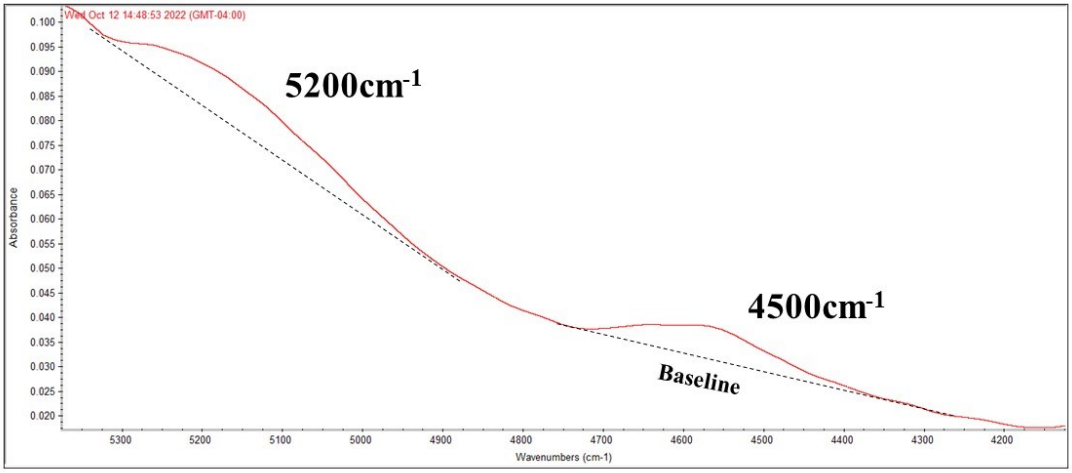

Figure 1: Example of an infrared spectrum showing the OH peak at 4500cm^{-1} and the H_2O_{dm} peak at 5200cm^{-1}. Sample RBC-862: A-1/Niv 14/Sur.

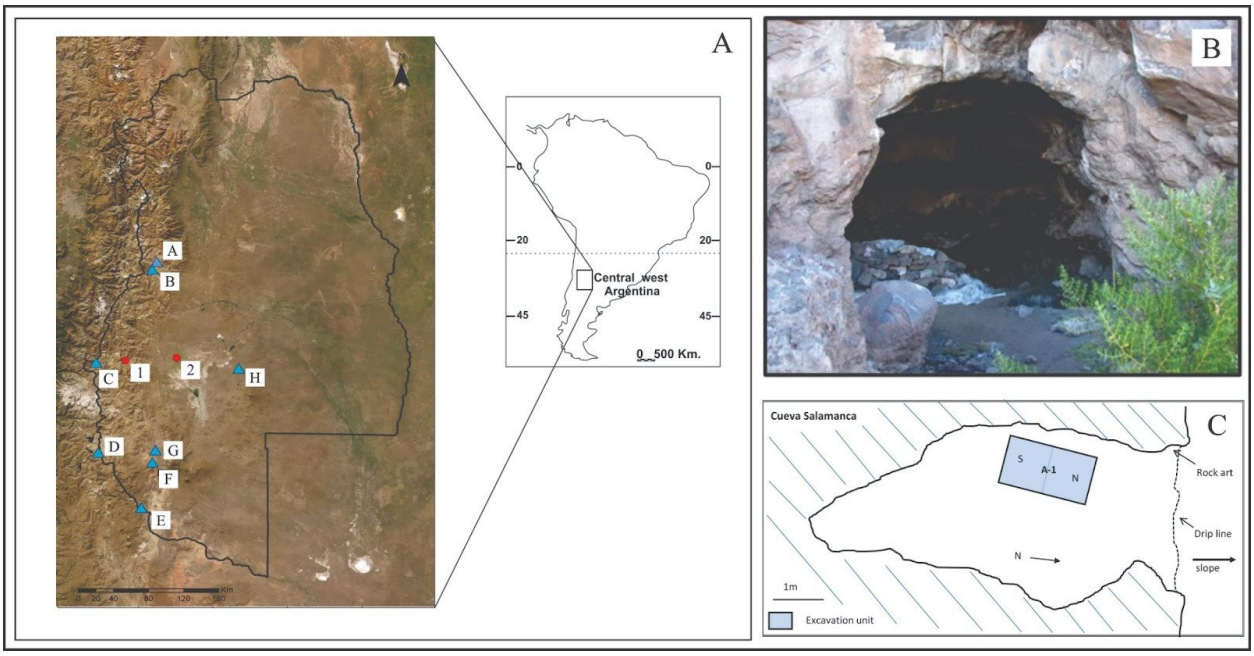

Figure 2. A: Map of Mendoza province with archaeological sites: 1. El Desecho, 2. Salamanca cave, and obsidian geological sources: A. Paramillos, B. Laguna del Diamante, C. Las Cargas, D. Maule 1, E. Maule 2, F. Zaino, G. Coche Quemado, and H. El Peceño. B: Salamanca Cave exterior. The entrance is about 2.75m wide and 3m high. C: Top plan of Salamanca Cave with the test unit location.

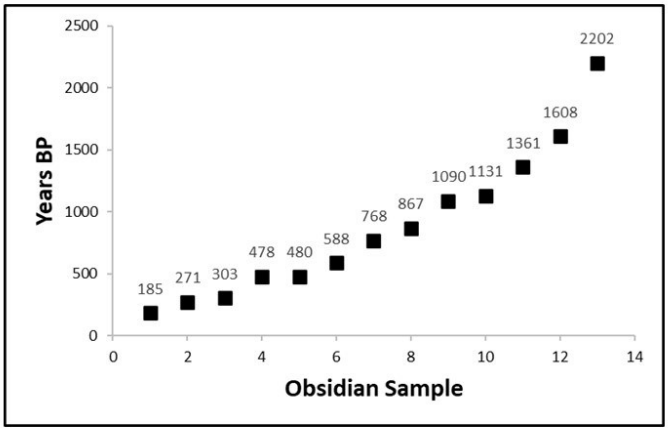

Figure 3. OHD ages computed for Salamanca Cave obsidian specimens. The sample surrounded by a red circle shows evidence of surface pitting.

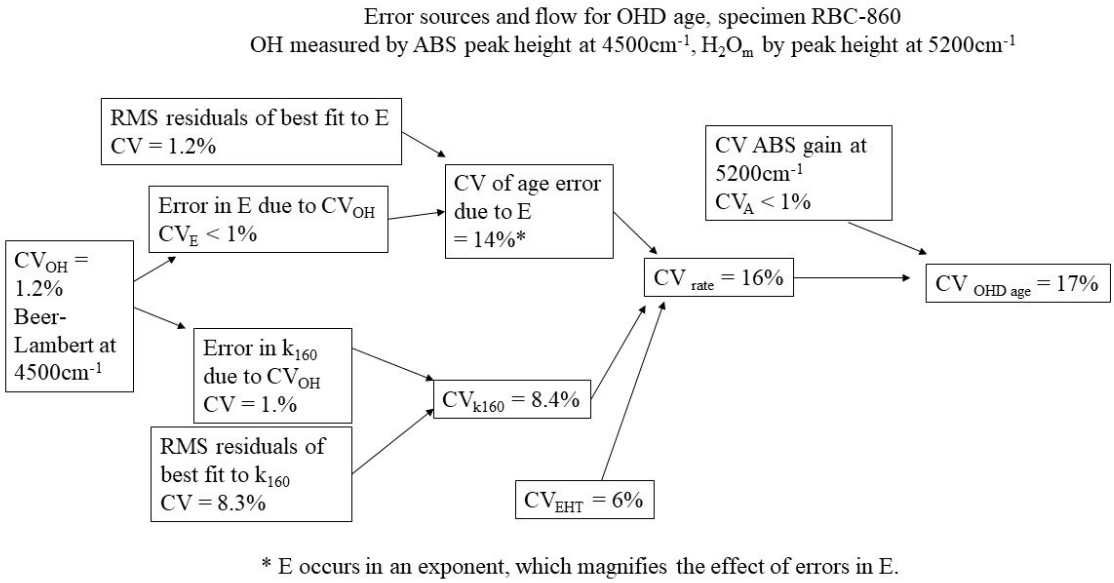

Figure 4: Error sources for OHD age estimates (Specimen RBC-860) measuring the hydroxyl (OH) peak height at 4500cm^{-1}and the H_2O_{dm} peak height at 5200cm^{-1}. (Term abbreviations: CV= Coefficient of Variation; RMS=Root Mean Square).